Quest Journals
Journal of Architecture and Civil Engineering
Volume 7 ~ Issue 5 (2022) pp: 23-31
ISSN(Online) : 2321-8193
www.questjournals.org

Research Paper

The Integration of Image-Based Navigation & GPS Carrier Phase Delta Positioning for Aerial Triangulation using Low-Cost Drones with Limited Number of Ground Control Points

Mustafa M. Amami
Civil Engineering Department, Benghazi University, Libya
Corresponding Author: Mustafa M. Amami

ABSTRACT: *In this paper, the integration of Image-Based Navigation/GPS Delta Positioning (GPS-DP) is tested and evaluated for investigating the possibility of carrying out Aerial Triangulation (AT) using low-cost drone with limited number of GCP's. 98 overlapped aerial images, taken by DJI Mavic 2 PRO drone, with Hasselblad L1D-20C 20 MP camera & UHD video, from 350 m height, with 8.5 cm ground pixel footprint are used in this paper, for covering nearly 15 km route. Self-developed Matlab algorithms, Leica Geo Office (LGO) and Leica Photogrammetric Suite (LPS) software has been used for applying IBN/GPS-DP integration and evaluating the results. Different number of Ground Control Points (GPS) and intervals have been used for reliable evaluation of the possibility of reducing the required number of GCP's along the trajectory. Tests have included utilizing only 6 GCP's, distributed as two equal groups on the two sides of the route, and 9 GCP's, distributed as 3 equal groups with intervals of 7.5 Km. The obtained results of these two trails have been compared to the quality of the Object Space Coordinates (OSC's) that obtained using 30 GCP's distributed well along the route without the integration of IBN/GPS-DP. The results show that employing the integration of IBN/GPS-DP in AT has on the whole reduced considerably the high-need of GCP's along the trajectory for low-cost drones. The quality of OSC's with the 9 GCP's test has reached the level of less than 1 & 2 decimeters in horizontal and vertical, respectively, which are very close to that obtained without the integration of IBN/GPS-DP, using 30 well-distributed GCP's with interval of 0.5 Km. Tests show that the quality of OSC's decreases as moving away from the GCP's, reaching the minimum level nearly in the middle of intervals. With 15 Km interval, the quality of OSC's has relatively been degraded, especially in the middle of trajectory, where IBN and GPS-DP are error cumulative techniques and require correction after a number of images and time, respectively. For increasing the quality of results, reducing the required number of GCS's, and increasing the GCS's intervals, it is recommended to increase the accuracy of IBN using higher camera resolutions, bigger focal lengths, smaller pixel sizes, and less flying height. Also, carrier phase of GPS+GLONASS observables can be used instead of GPS alone for more reliable and dependable DP. Self-Calibration Bundle Block Adjustment (SCBBA) with additional camera calibration parameters can also be investigated for more precise results. To end with, the integration of IBN/GPS-DP has shown a high ability to reduce considerably the high-need of GCP's in AT using low-cost drones, which helps to carry out the aerial photogrammetric works in unreachable or partially accessible areas, reducing cost, effort, and time.*

KEYWORDS: *Low-cost drone; GPS delta positioning; aerial images-based navigation; low-number of ground control points.*

R*eceived 05 May, 2022;* ***R****evised 17 May, 2022;* ***A****ccepted 19 May, 2022* © *The author(s) 2022.*
P*ublished with open access at* ***www.questjournals.org***

I. INTRODUCTION

Photogrammetry can be defined as the technique, by which measurements from different types of photos can be taken, including aerial, space and terrestrial images [1]. These days, the applications of photogrammetry is used extensively in a wide range of scientific areas, such as topographic mapping, construction monitoring, engineering geology, medication, safety and security, urban planning and management, robot navigation, water-bodies monitoring, and Geographic Information System (GIS) data collection [2].

Using high-resolution images, accurate geo-referencing techniques, precise Automatic Image Matching (AIM) techniques, and suitable statistical testing and efficient filters, photogrammetry can provide high-quality real data [3]. Photogrammetry overcomes the conventional surveying techniques in terms of saving time, cost, and efforts, and it's a high-ability to cover unreachable, challenging, risky, and hazardous zones. This is of course behind the main strong point which is providing final 3D products with real and detailed views. Photogrammetry, on the other hand, needs high-level understanding and training to reach the desired goals, where the site and processing steps may not be difficult in terms of efforts, but complicated in terms of planning, programming, and details [4]. The other main drawback is the high-need of Ground Control Points (GCP) for precise and robust geometry of Self Calibration Bundle Block Adjustment (SCBBA), especially when the observed Exterior Orientation Parameters (EOP) are not reliable because of using stand-alone GPS receivers or the integration of low-cost GPS/Inertial Navigation Systems (INS) [5]. These days, drones are used progressively in photogrammetry for providing ortho-mosaics, Digital Elevation Models (DEM), land detailed surveying and topographic mapping. Drones that are designed specifically for engineering surveying and photogrammetric applications tend to be high-priced, as they provided with special features, including high-resolution metric cameras, high-quality Real Time Kinematic (RTK)-GPS/INS integrated system [3] [4]. Examples of the famous surveying drones are Wingtra-One GEN II, DJI Phantom 4 RTK, and DJI Matrice 300 RTK [4]. Low-cost drones that are designed for unprofessional intentions can also be used for photogrammetric applications, and the quality of outcomes depends on the quality of the navigation and vision sensors used. Example of up-to-date low-cost drones that have become progressively used in photogrammetric applications is DJI Mavic 2 PRO drone. Even though high-quality surveying drones can depend only on the obtained high-accurate EOP's and stable Interior Orientation Elements (IOE) for generating the required photogrammetric products, a number of GCP's tend to be used for more robust and stable geometry. With low-cost drones, utilizing GCP's is highly-essential for reliable results, where stand-alone GPS code positioning with accuracy of a few meters tends to be used for determining the camera EOP's. The high-need of GCP's is costly, time-consuming and may not be possible in some inaccessible areas.

Image-Based Navigation (IBN) is a positioning technique that is based on photos, which is also known as vision-based navigation and Simultaneous Localization And Mapping (SLAM) in computer and robot sciences [6]. In general, there are three main steps in IBN, namely intersection, resection, and compound case which is known as Aerial Triangulation (AT). In intersection solution, the camera EOP's in at least two overlapped images are known and the aim is to determine the Object Space Coordinates (OSC) of any item appear in the overlapping area. Each common point forms 4 co-linearity equations in just 3 unknowns, which are the OSC's of this point. In aerial resection, the EOP's of the two images are unknowns and should be determined based on GCP's. At least 3 GCP's, that appear in each photo, can be used for determining the 6 EOP's of each image (3D camera center position & 3D rotations), and the overlapping between images is not necessary, where each image can be solved individually. More than 3 well-distributed GCP's are recommended to be used and solved using Least Squares Method (LSM) for reliable and dependable results. AT includes both intersection and resection solutions in an open number of overlapped images, where all observations are bundled in one SCBBA. Relative Orientation (RO) is another type of AT, in which all the observations are considered as unknowns with the exception of the EOP's of one image which are regarded as fixed values (usually zeros), and bundled together in SCBBA. All the results of RO are relative to the EOP's of the fixed image and can be transformed to absolute values using at least 3 GCP's [6]. IBN starts with resection based on a few GCP's to determine the cameras EOP's, moving to interaction to determine the OSC's of some matched common points based on the determined EOP's in the previous step, returning back to resection for determining the EOP's of the new images, and so on. If the procedure is carried out in real time for determining the drone positioning, there will be no chance for applying SCBBA for the whole observations from the first image until the last one. However, in post processing cases, there will be a possibility for applying SCBBA for all observations including another group of GCP's at the end of the track to band any drifts in IBN. Errors in IBN is cumulative and increase over time, especially if the processing is controlled by GCP's from one end only and free from the other end. In case of two-side controlled IBN, the errors can be reduced using SCBBA, where all observations are bundled together, adjusted and corrected, giving more precise results. In long routes, even with two-end controlled SCBBA, the errors will be significant in the areas away from the GCP's; thus, in-between GCP's can be used for better results. Tests and experiments show that the number of GCP's required for precise IBN depends significantly of the quality of the initial values of EOP's used in SCBBA and their standard deviation values, where the more precise EOP's, the less GCP's needed from accurate products [2]. Based on that, considerable number of GCP's is essential with low-cost drones in surveying works, where single frequency low-cost GPS receivers tend to be used, providing low-quality EPO's [7][8], which make the SCBBA unstable and geometrically weak.

However, beside the stand-alone code positioning, low-cost GPS receivers can provide carrier phase observables [9]. Stand-alone double differences carrier phase, known also as GPS Delta Positioning (GPS-DP),

is the most accurate stand-alone velocity estimation technique based on single frequency stand-alone GPS carrier phase observables. Precise GPS relative positioning can then be achieved by integrating the velocity over epoch. DP is a double differences technique including two epochs, two satellites and one receiver. In GPS-DP, the ambiguity and receiver clock errors are eliminated, whereas satellite clock error, orbit errors, and ionosphere and tropospheric delays are lowered meaningfully based on the high correlation between these errors over short time. Multipath effect remains and can be reduced to some extent based on the multipath correlation over time, whereas receiver noise increases and cumulated [10]. Loosely coupled integration between GPS-DP and stand-alone GPS code positioning can be applied to enhance the performance of low-cost GPS receivers [9]. Also, GPS-DP can be integrated with MEMS-Based INS for precise low-coat navigation using Kalman filter [10] The main weakness of GPS-DP is its dependence, where just relative shifts can be determined. Error growing is another drawback of GPS-DP, where the shifts are determined for each epoch individually, and added to the previous shifts for obtaining the present relative location. Moreover, GPS-DP is susceptible to cycle slips, and at least 3 GPS satellites should be observed between each two adjacent epochs for determining cycle slips-free stand-alone double differences carrier phase solution [11] [12].

In this paper, the integration between IBN and GPS-DP is investigated, tested and evaluated for enhancing low-cost drone navigation and reducing the number of GCP's required for robust SCBBA. IBN equations and steps will be illustrated firstly. Then, the derivation of GPS-DP equations will be explained, and finally, the integration between the two techniques will be shown as a diagram. All the required data in this paper has been taken from and based on [4], in which DJI Mavic 2 PRO drone, with 20 MP camera & Ultra-High-Definition (UHD) video, has been used for covering nearly 15 km route, with 98 overlapped images, taken from 350 m height and 8 cm ground pixel footprint. The drone has been adjusted by the research group of this paper to record GPS carrier phase observations based on u-blox GPS chip. 60 precise GCP's and check points are available in the site, which has been used in the desired manner in this paper. All the essential planning, flight mission calculations, camera calibration, fixing GCP's & check points, camera time intervals, flight speed, camera settings and overlapping rates have been explained in details in [4], and just summarized in this paper. Self-developed Matlab algorithms, Leica Geo Office (LGO) and Leica Photogrammetric Suite (LPS) software are used for carrying out the suggested integration, processing the collected data, and evaluating the results.

II. MATHEMATICAL DESCRIPTION

2.1- IMAGE-BASED NAVIGATION (IBN)

IBN depends completely on photogrammetric co-linearity equations, which include the IOE's of used camera (focal length & principal point coordinates), the EOP's of each image (3D coordinates of the capturing station and 3D rotations about the image axes), 2D image coordinates of objects, and 3D OSC's. Co-linearity equations are nonlinear and need to be linearized to be used with LSM. As explained in the introduction, IBN can be divided into two steps in real time applications, which are resection and intersection, and 3 steps in post processing cases, which are resection, intersection, and AT using SCBBA. Co-linearity equations and linearization can be illustrated as following:

$$F = xa = x_0 - f\frac{m_{11}(X_A - X_L) + m_{12}(Y_A - Y_L) + m_{13}(Z_A - Z_L)}{m_{31}(X_A - X_L) + m_{32}(Y_A - Y_L) + m_{33}(Z_A - Z_L)}$$

$$G = Ya = y_0 - f\frac{m_{21}(X_A - X_L) + m_{22}(Y_A - Y_L) + m_{23}(Z_A - Z_L)}{m_{31}(X_A - X_L) + m_{32}(Y_A - Y_L) + m_{33}(Z_A - Z_L)}$$

Where,

$(x_0, y_0), f$	*Principle point coordinates & focal length*
xa, ya	*Object image coordinates of point a*
X_A, Y_A, Z_A	*Objects space coordinates of point A*
X_L, Y_L, Z_L	*Capturing point coordinates*
$m_{11}....m_{33}$	*Elements of 3D conformal coordinate transformation Cos matrix includes* (ω, φ, k)
(ω, φ, k)	*The rotations of the camera about X, Y, & Z axes*

These two equations can be generally linearized using Taylor's theorem as following:

$$F_0 + \left(\frac{\partial F}{\partial f}\right)_0 df + \left(\frac{\partial F}{\partial x_0}\right)_0 dx_0 + \left(\frac{\partial F}{\partial y_0}\right)_0 dy_0 + \left(\frac{\partial F}{\partial \omega}\right)_0 d\omega + \left(\frac{\partial F}{\partial \varphi}\right)_0 d\varphi + \left(\frac{\partial F}{\partial k}\right)_0 dk + \left(\frac{\partial F}{\partial X_A}\right)_0 dX_A + \left(\frac{\partial F}{\partial Y_A}\right)_0 dY_A + \left(\frac{\partial F}{\partial Z_A}\right)_0 dZ_A + \left(\frac{\partial F}{\partial X_L}\right)_0 dX_L + \left(\frac{\partial F}{\partial Y_L}\right)_0 dY_L + \left(\frac{\partial F}{\partial Z_L}\right)_0 dZ_L = xa$$

$$G_0 + \left(\frac{\partial G}{\partial f}\right)_0 df + \left(\frac{\partial G}{\partial x_0}\right)_0 dx_0 + \left(\frac{\partial G}{\partial y_0}\right)_0 dy_0 + \left(\frac{\partial G}{\partial \omega}\right)_0 d\omega + \left(\frac{\partial G}{\partial \varphi}\right)_0 d\varphi + \left(\frac{\partial G}{\partial k}\right)_0 dk + \left(\frac{\partial G}{\partial X_A}\right)_0 dX_A + \left(\frac{\partial G}{\partial Y_A}\right)_0 dY_A + \left(\frac{\partial G}{\partial Z_A}\right)_0 dZ_A + \left(\frac{\partial G}{\partial X_L}\right)_0 dX_L + \left(\frac{\partial G}{\partial Y_L}\right)_0 dY_L + \left(\frac{\partial G}{\partial Z_L}\right)_0 dZ_L = ya$$

Where,

F_0, G_0	*The values of the equation with the initial values used for the unknowns*
$(\partial F)_0$, $(\partial G)_0$	*The values of the differentiation of the equation with respect of each unknown using the initial values of unknowns*
df, dx_0, ...	*The differences between computed and most probable values of each unknowns*

In the first step of IBN, which is photogrammetric resection, image coordinates (x_a, y_a) are measured values, OSC's (X_A, Y_A, Z_A) are known, EOP's (X_L, Y_L, Z_L, ω, φ, k) are unknown. If the camera IOE's (f, x_0, y_0) are known, at least 3 GCP's should be known, and if the IOE's are unknown or not reliable, at least 4 GCP's should be in use. With (n) number of GCP's and (m) number of overlapped images, the equations of the IBN's first step with known IOE's can be written as following, where the number of equations is (2 * n * m) and the number of unknowns is (6 * m):

$$\left(\frac{\partial F_{1:n}}{\partial \omega_{1:m}}\right)_0 d\omega_{1:m} + \left(\frac{\partial F_{1:n}}{\partial \varphi_{1:m}}\right)_0 d\varphi_{1:m} + \left(\frac{\partial F_{1:n}}{\partial k_{1:m}}\right)_0 dk_{1:m} + \left(\frac{\partial F_{1:n}}{\partial X_{L\,1:m}}\right)_0 dX_{L\,1:m} + \left(\frac{\partial F_{1:n}}{\partial Y_{L\,1:m}}\right)_0 dY_{L\,1:m} + \left(\frac{\partial F_{1:n}}{\partial Z_{L\,1:m}}\right)_0 dZ_{L\,1:m} = xa_{1:n} - F_{0\,1:n}$$

$$\left(\frac{\partial G_{1:n}}{\partial \omega_{1:m}}\right)_0 d\omega_{1:m} + \left(\frac{\partial G_{1:n}}{\partial \varphi_{1:m}}\right)_0 d\varphi_{1:m} + \left(\frac{\partial G_{1:n}}{\partial k_{1:m}}\right)_0 dk_{1:m} + \left(\frac{\partial G_{1:n}}{\partial X_{L\,1:m}}\right)_0 dX_{L\,1:m} + \left(\frac{\partial G_{1:n}}{\partial Y_{L\,1:m}}\right)_0 dY_{L\,1:m} + \left(\frac{\partial G_{1:n}}{\partial Z_{L\,1:m}}\right)_0 dZ_{L\,1:m} = ya_{1:n} - G_{0\,1:n}$$

And with unknown IOE's of (r) number of cameras, the equations can be written as following, where the number of equations is (2 * n * m) and the number of unknowns is (3 * r + 6 * m):

$$\left(\frac{\partial F_{1:n}}{\partial f_{1:r}}\right)_0 df_{1:r} + \left(\frac{\partial F_{1:n}}{\partial x0_{1:r}}\right)_0 dx0_{1:r} + \left(\frac{\partial F_{1:n}}{\partial y0_{1:r}}\right)_0 dy0_{1:r} + \left(\frac{\partial F_{1:n}}{\partial \omega_{1:m}}\right)_0 d\omega_{1:m} + \left(\frac{\partial F_{1:n}}{\partial \varphi_{1:m}}\right)_0 d\varphi_{1:m} + \left(\frac{\partial F_{1:n}}{\partial k_{1:m}}\right)_0 dk_{1:m} + \left(\frac{\partial F_{1:n}}{\partial X_{L\,1:m}}\right)_0 dX_{L\,1:m} + \left(\frac{\partial F_{1:n}}{\partial Y_{L\,1:m}}\right)_0 dY_{L\,1:m} + \left(\frac{\partial F_{1:n}}{\partial Z_{L\,1:m}}\right)_0 dZ_{L\,1:m} = xa_{1:n} - F_{0\,1:n}$$

$$\left(\frac{\partial G_{1:n}}{\partial f_{1:r}}\right)_0 df_{1:r} + \left(\frac{\partial G_{1:n}}{\partial x0_{1:r}}\right)_0 dx0_{1:r} + \left(\frac{\partial G_{1:n}}{\partial y0_{1:r}}\right)_0 dy0_{1:r} + \left(\frac{\partial G_{1:n}}{\partial \omega_{1:m}}\right)_0 d\omega_{1:m} + \left(\frac{\partial G_{1:n}}{\partial \varphi_{1:m}}\right)_0 d\varphi_{1:m} + \left(\frac{\partial G_{1:n}}{\partial k_{1:m}}\right)_0 dk_{1:m} + \left(\frac{\partial G_{1:n}}{\partial X_{L\,1:m}}\right)_0 dX_{L\,1:m} + \left(\frac{\partial G_{1:n}}{\partial Y_{L\,1:m}}\right)_0 dY_{L\,1:m} + \left(\frac{\partial G_{1:n}}{\partial Z_{L\,1:m}}\right)_0 dZ_{L\,1:m} = ya_{1:n} - G_{0\,1:n}$$

In the second step of IBN, which is photogrammetric intersection, image coordinates (x_a, y_a) are measured values, OSC's (X_A, Y_A, Z_A) are unknown, EOP's (X_L, Y_L, Z_L, ω, φ, k) of two overlapping images are known. If the camera IOE's (f, x_0, y_0) are known, the OSC's of each measured point on the overlapping area between the two images can be determined individually, where 4 co-linearity equations are formed in 3 unknowns. If the IOE's are unknown or not reliable, at least 3 overlapped points should be used where each point can take one of the 3 IOE's. The equations of the IBN's second step with known IOE's, (n) number of OSC's and (m) number of overlapped images can be written as following, where the number of equations is (2 * n * m) and the number of unknowns is (3 * n):

$$\left[\left(\frac{\partial F_{1:n}}{\partial X_{1:n}}\right)_0 dX_{1:n} + \left(\frac{\partial F_{1:n}}{\partial Y_{1:n}}\right)_0 dY_{1:n} + \left(\frac{\partial F_{1:n}}{\partial Z_{1:n}}\right)_0 dZ_{1:n} = xa_{1:n} - F_{0\,1:n}\right]_{1:m}$$

$$\left[\left(\frac{\partial G_{1:n}}{\partial X_{1:n}}\right)_0 dX_{1:n} + \left(\frac{\partial G_{1:n}}{\partial Y_{1:n}}\right)_0 dY_{1:n} + \left(\frac{\partial G_{1:n}}{\partial Z_{1:n}}\right)_0 dZ_{1:n} = ya_{1:n} - G_{0\,1:n}\right]_{1:m}$$

And with unknown IOE's of (r) number of cameras, the equations can be written as following, where the number of equations is (2 * n * m) and the number of unknowns is (3 * n + 3 * r):

$$\left[\left(\frac{\partial F_{1:n}}{\partial f_{1:r}}\right)_0 df_{1:r} + \left(\frac{\partial F_{1:n}}{\partial x0_{1:r}}\right)_0 dx0_{1:r} + \left(\frac{\partial F_{1:n}}{\partial y0_{1:r}}\right)_0 dy0_{1:r} + \left(\frac{\partial F_{1:n}}{\partial X_{1:n}}\right)_0 dX_{1:n}{}_0 + \left(\frac{\partial F_{1:n}}{\partial Y_{1:n}}\right)_0 dY_{1:n} + \left(\frac{\partial F_{1:n}}{\partial Z_{1:n}}\right)_0 dZ_{1:n} = xa_{1:n} - F_{0\,1:n}\right]_{1:m}$$

$$\left[\left(\frac{\partial G_{1:n}}{\partial f_{1:r}}\right)_0 df_{1:r} + \left(\frac{\partial G_{1:n}}{\partial x0_{1:r}}\right)_0 dx0_{1:r} + \left(\frac{\partial G_{1:n}}{\partial y0_{1:r}}\right)_0 dy0_{1:r} + \left(\frac{\partial G_{1:n}}{\partial X_{1:n}}\right)_0 dX_{1:n}{}_0 + \left(\frac{\partial G_{1:n}}{\partial Y_{1:n}}\right)_0 dY_{1:n} + \left(\frac{\partial G_{1:n}}{\partial Z_{1:n}}\right)_0 dZ_{1:n} = ya_{1:n} - G_{0\,1:n}\right]_{1:m}$$

In AT, the results of the two previous steps are used as initial values with weights that are based on the standard deviation values obtained from the covariance matrix of LSM. This includes image coordinates (x_a, y_a) for all points, OSC's (X_A, Y_A, Z_A) of all points, EOP's (X_L, Y_L, Z_L, ω, φ, k) of all images, and IOE's (f, x_0, y_0) of used cameras. The general formulas of AT equations for (n) image points, (m) images, and (r) cameras can be written as:

$$\left(\frac{\partial F_{1:n}}{\partial f_{1:r}}\right)_0 df_{1:r} + \left(\frac{\partial F_{1:n}}{\partial x0_{1:r}}\right)_0 dx0_{1:r} + \left(\frac{\partial F_{1:n}}{\partial y0_{1:r}}\right)_0 dy0_{1:r} + \left(\frac{\partial F_{1:n}}{\partial X_{1:n}}\right)_0 dX_{1:n} + \left(\frac{\partial F_{1:n}}{\partial Y_{1:n}}\right)_0 dY_{1:n} + \left(\frac{\partial F_{1:n}}{\partial Z_{1:n}}\right)_0 dZ_{1:n} + \left(\frac{\partial F_{1:n}}{\partial \omega_{1:m}}\right)_0 d\omega_{1:m} + \left(\frac{\partial F_{1:n}}{\partial \varphi_{1:m}}\right)_0 d\varphi_{1:m} + \left(\frac{\partial F_{1:n}}{\partial k_{1:m}}\right)_0 dk_{1:m} + \left(\frac{\partial F_{1:n}}{\partial X_{L\,1:m}}\right)_0 dX_{L\,1:m} + \left(\frac{\partial F_{1:n}}{\partial Y_{L\,1:m}}\right)_0 dY_{L\,1:m} + \left(\frac{\partial F_{1:n}}{\partial Z_{L\,1:m}}\right)_0 dZ_{L\,1:m} = xa_{1:n} - F_{0\,1:n}$$

$$\left(\frac{\partial G_{1:n}}{\partial f_{1:r}}\right)_0 df_{1:r} + \left(\frac{\partial G_{1:n}}{\partial x0_{1:r}}\right)_0 dx0_{1:r} + \left(\frac{\partial G_{1:n}}{\partial y0_{1:r}}\right)_0 dy0_{1:r} + \left(\frac{\partial G_{1:n}}{\partial X_{1:n}}\right)_0 dX_{1:n} + \left(\frac{\partial G_{1:n}}{\partial Y_{1:n}}\right)_0 dY_{1:n} + \left(\frac{\partial G_{1:n}}{\partial Z_{1:n}}\right)_0 dZ_{1:n} + \left(\frac{\partial G_{1:n}}{\partial \omega_{1:m}}\right)_0 d\omega_{1:m} + \left(\frac{\partial G_{1:n}}{\partial \varphi_{1:m}}\right)_0 d\varphi_{1:m} + \left(\frac{\partial G_{1:n}}{\partial k_{1:m}}\right)_0 dk_{1:m} + \left(\frac{\partial G_{1:n}}{\partial X_{L\,1:m}}\right)_0 dX_{L\,1:m} + \left(\frac{\partial G_{1:n}}{\partial Y_{L\,1:m}}\right)_0 dY_{L\,1:m} + \left(\frac{\partial G_{1:n}}{\partial Z_{L\,1:m}}\right)_0 dZ_{L\,1:m} = ya_{1:n} - G_{0\,1:n}$$

All previous equations can be solved using LSM, which can provide useful statistical information beside the final solution, such as the standard deviation of observations and unknowns. In the case of real time processing, just sequential resection and intersection steps can be used and there will be no chance for adjusting the whole observations and unknowns in one SCBBA solution like in the case of post processing. Without

SCBBA solution, the errors in drone positioning will be cumulative, where all errors in the GCP's, image points, and IOE's will be reflected directly on the EOP's of the drone.

2.2- GPS DELTA POSITIONING (GPS-DP)

GPS carrier phase equation can be written as [9]:

$$CP_{(s,r)(k)} = p_{(s,r)(k)} + c(\,dT_{(s)(k)} - dt_{(r)(k)}\,) + dion_{(s,r)(k)} + dtrop_{(s,r)(k)} + dor_{(s)(k)} + E_{(s,r)(k)} + L * N$$

Where,

$CP_{(s,r)(k)}$	*the carrier phase observation (m)*
$p_{(s,r)(k)}$	*the true range between receiver (r) and satellite (s) at epoch (k)*
c	*the speed of light*
$dT_{(s)(k)}$	*the clock error of satellite (s) at epoch (k)*
$dt_{(r)(k)}$	*the clock error of receiver (r) at epoch (k)*
$dion_{(s,r)(k)}$	*the ionospheric delay error between receiver (r) and satellite (s) at epoch (k) (m)*
$dtrop_{(s,r)(k)}$	*the tropospheric delay error between receiver (r) and satellite (s) at epoch (k) (m)*
$dor_{(s)(k)}$	*the orbit error of satellite (s) at epoch (k) (m)*
$E_{(s,r)(k)}$	*the measurement noise including multipath between receiver (r) and satellite (s) at epoch (k)*
L	*the carrier wavelength (m)*
N	*the unknown integer ambiguity (cycle)*

The true range between receiver *(r)* and satellite *(s)* at epoch *(k)* can be written as:

$$p_{(s,r)(k)} = ((X_{(s)} - X_{(r)})^2 + ((Y_{(s)} - Y_{(r)})^2 + ((Z_{(s)} - Z_{(r)})^2)^{0.5}$$

Where, *X, Y* and *Z* are the satellite and receiver Cartesian coordinates.

In GPS-DP, the first single differencing is formed between one receiver (r), one satellite (s) and two adjacent epochs *$((k)$ & $(k+1)$).* The single differencing equation can be written as:

$$SD_{(s)(r)(k+1,k)} = CP_{(s,r)(k+1)} - CP_{(s,r)(k)}$$

$$\left[p_{(s,r)(k+1)} + c\left(dT_{(s)(k+1)} - dt_{(r)(k+1)}\right) + dion_{(s,r)(k+1)} + dtrop_{(s,r)(k+1)} + dor_{(s)(k+1)} + E_{(s)(r)(k+1)} + L * N\right]$$

$$-\left[p_{(s,r)(k)} + c\left(dT_{(s)(k+1)} - dt_{(r)(k)}\right) + dion_{(s,r)(k)} + dtrop_{(s,r)(k)} + dor_{(s)(k)} + E_{(s)(r)(k)} + L * N\right]$$

Where, $SD_{(s)(r)(k+1,k)}$ is single differencing between receiver (r), one satellite (s) and two adjacent epochs *((k) & $(k+1)$)*

From the single differences, the double difference ambiguity is removed as long as the integer ambiguity remains constant and the receiver keeps lock the satellite signal. Satellite clock error is reduced based on the stability of the satellite clock over transmission times. Satellite orbit errors are reduced significantly based on the high correlation between the satellite orbit errors over time. Ionosphere and troposphere errors are reduced to the change in delay across the interval. Multipath remains and can be reduced based on the multipath correlation over time. However, receiver clock error is doubled and receiver measurements noise increases [10]. The final formula of single differences equation can be written as:

$$SD_{(s)(r)(k+1,k)} = p_{(s)(r)(k+1,k)} - c\,dt_{(r)(k+1,k)} + E_{(s)(r)(k+1,k)}$$

The second differencing in GPS-DP is carried out between two single differences, similar to that in equation (3), cross two satellites (s) and (j). This can be written as:

$$DD_{(s,j)(r)(k+1,k)} = SD_{(s)(r)(k+1,k)} - SD_{(j)(r)(k+1,k)}$$

$$p_{(s)(r)(k+1,k)} - c\,dt_{(r)(k+1,k)} + E_{(s)(r)(k+1,k)} - p_{(j)(r)(k+1,k)} + c\,dt_{(r)(k+1,k)} - E_{(j)(r)(k+1,k)}$$

Where, $DD_{(s,j)(r)(k+1,k)}$ is double differences between one receiver *(r),* two epochs *(k+1)* & *(k),* and two satellites *(s)* & *(j).*

Receiver clock error is cancelled out in the double differences. This is extremely important for getting accurate results where the oscillators in low cost receivers vary in frequency with temperature and pressure making the receiver clock unreliable. The final formula of double differences equation can be written as:

$$DD_{(s,j)(r)(k+1,k)} = p_{(s,j)(r)(k+1,k)} + E_{(s,j)(r)(k+1,k)}$$

The only unknowns in this equation are the receiver Cartesian coordinates in the two epochs *(k)* & *(k+1).* The changes in the receiver positions between the two epochs can be determined by fixing the coordinated of the receiver at epoch *(k)* (as zeros for example) and solving for the receiver coordinated at epoch *(k+1).* To determine the relative position of the receiver at epoch *(k + 1)* from *(k),* the double differences equation should be written as:

$$b = A\,X + v$$

Where,

b	the measurement victor with a size of (number of epochs -1, 1)
X	the parameter victor with a size of (number of epochs * 3, 1) which include the change in Cartesian position
A	matrix with a size of (number of epoch -1, number of epoch * 3) which relates the parameters to the states
v	a vector of random noise with a size of (number of epochs -1, 1)

This equation can then be solved by LSM as:

$$X = (A^T\,w\,A)^{-1}\,A^T\,w\,b$$

Where,

w	the weight matrix with a size of (number of epochs -1, number of epochs -1) which is based on the average satellite residuals obtained from the stand alone code positioning calculations.

2.3- THE INTEGRATION OF IBN/GPS-DP

The integration of IBN and GPS-DP can be summarized in figures (1), showing and illustrating the forward, reverse & final integration steps.

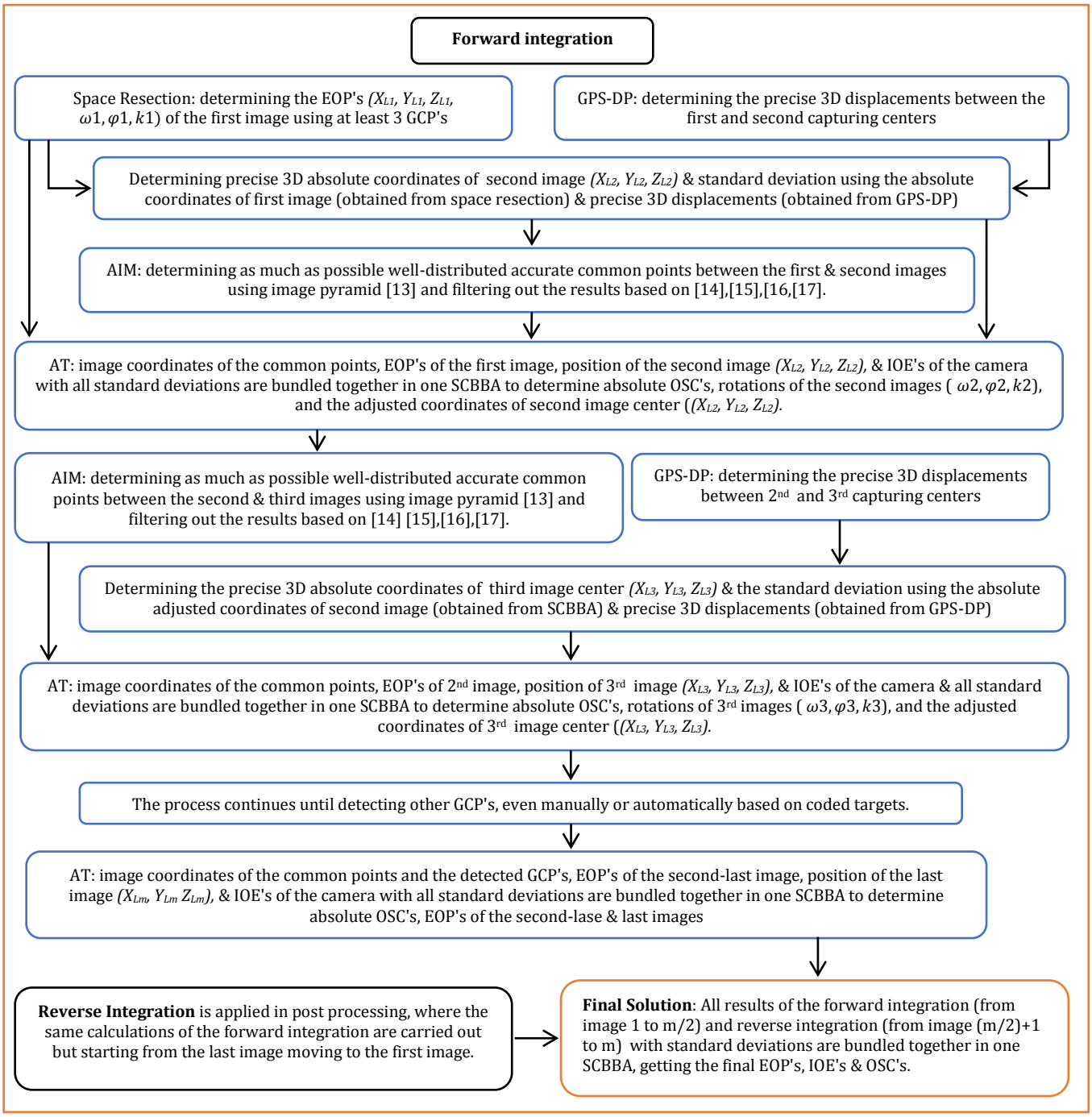

Figure 1: the integration of IBN/GPS-DP

III. TESTING DATA & EVALUATION METHOD

As mentioned before, all testing data used in this paper is based on [4], in which DJI Mavic 2 PRO drone, provided by Hasselblad L1D-20C camera, has been used for creating Digital Elevation Model (DEM) and carrying out topographic surveying for an area of 15 km long and 200 m wide. The route has been chosen by the exploration team in the owner company as an preliminary route for gas and oil pipeline between manifold station and oil & gas refining and processing plant. The site is an empty desert area located in the South of Libya and fully with sand dunes that fluctuate in elevations significantly. The data has been collected by the surveying team at Benghazi University, Civil Engineering Department for the benefit of a local oil and gas company. The drone is provided with low-cost GPS receiver with circle patch antenna for navigating the drone in horizontal and vertical direction with accuracy of a few meters in open-sky and multipath-free environments [8]. Triple frequency Leica GS10 GNSS system has been used in this project for fixing 60 GCP's and check points along the trajectory with intervals of 500 m. GNSS data has been processed as static carrier phase

Differential GNSS (DGNSS) technique and based on 6 hours Precise Point Positioning (PPP) reference point. The GNSS collected data has been processed using LGO software, and the final obtained coordinates as well as the standard deviation values have been used in the SCBBA calculations in this paper. As for the flight mission calculations, see [3], [4]. Table (1) illustrates the whole information of the drone, camera, calibration results, and flight mission features.

Table 1: The whole details of drone, camera, & flight mission features

Hasselblad L1D-20C Camera		DJI Mavic 2 PRO	
Sensor	1" CMOS	Takeoff Weight	907 g
Focal length	Actual: 10.3 mm	Dimensions	Folded: 214 × 91 × 84 mm
Best ISO value	100	Max speed (no wind)	72 K/h
Shutter speed	8–1/8000 s	Max flight time (no wind)	31 min. (25 K/h)
Still image size	5472×3648	Max flight distance (no wind)	18 Km (50 K/h)
Resolution type	4K UHD	RTK possibility	No
Aperture size	f/2.8 – f/11	Max wind speed resistance	29 – 38 K/h
Video Quality	4k (30 F/s & 60 F/s)	Navigation	GPS+GLONASS
Effective pixels	20 MP	Exporting GNSS raw data	Yes (Adjusted)
Video F/s	30 F/s	Flying in specific tracks	Yes
Pixel size	2.4 micron	Pictures at specific locations	No
Camera Calibration			
Principle point x0	-0.1808 mm +/- 0.002 mm	Principle point y0	0.2602 mm +/- 0.002 mm
Calibrated Focal length		10.3099 mm+/- 0.004 mm	
Flying Mission Features			
Area	14860 m * 200 m	Number of flight lines	1
Pixel ground footprint	8 cm	Number of photos/Line	98
Flight height above MSH	350 m	Total number of photos	98
Scale	1:34000	Drone flight speed	10 km/h (2.8 m/s)
Image ground footprint	445 m * 295 m	Flight time	90 min. (3-4 batteries)
Air base	160 m	Camera time interval	Video (4k UHD)
Distance between flying lines	Just one flight line	Number of GCP's & check points	30 & 30
Actual wind speed	6 Km/h	Temperature	23 C^o
Whole area covered	15650 m * 295 m	Flight time	11:00 to 13:00 (30 min for changing batteries)

As for the evaluation method, the processing steps mentioned above will be applied firstly using only 3 GCP's at the beginning and other 3 by the end of the trajectory after 15 Km, and all GCP's and check points available along the route will be used as check points, where their coordinates will be calculated using the integration of IBN/GPS-DP and compared with the "true" values to determine absolute errors. For precise evaluation about the effect of the number of GCP's on the integration of IBN/GPS-DP, different intervals between the GCP's used in the processing have been used, including 15 Km & 7.5 Km. The results of utilizing 30 GCP's along the trajectory (every 0.5 Km) without the integration of IBN/GPS-DP which is applied in [4] has been also illustrated to help in the evaluation of the suggested integration. For example, with 7.5 Km interval, 3 groups of 3 GCP's will be used along the trajectory, one at the beginning, one in the middle, and the last by the end of the route. The results of the two intervals will be illustrated in one figure besides the reference results of the 0.5 Km to present the differences and the effect of the number and intervals between GCP's on the integration of IBN/GPS-DP.

IV. RESULTS & DISCUSSION

Figure (2) shows the whole results of the IBN/GPS-DP integration, including utilizing different GCP's intervals. From the figure it is clear that utilizing the suggested integration has in general reduced significantly the high-need of GCP's along the trajectory for low-cost drones. The quality of check points, with 0.5 Km GCP's intervals (30 GCP's) and without the integration of IBN/GPS-DP, has reached RMSE of 0.12 m & 0.18 cm in horizontal and vertical, respectively based on [4]. With IBN/GPS-DP integration and using only 6 GCP's; 3 at the beginning and 3 at the end of the trajectory, the absolute error of check points has reached 0.63 m and 0.91 m in horizontal and vertical, respectively as a maximum in nearly the middle of the trajectory, and averaged about 0.27 m and 0.41 m in horizontal and vertical, respectively as an overall average. It can be seen that the RMSE of check points increases as moving away from the start and end points, which include the GCP's, where the errors in the two integrated techniques, namely IBN and GPS-DP are cumulative and the only banding factor in this idea is observing the GCP's; thus, the greater the distance from the controlled areas, the bigger RMSE can be obtained. If the whole trajectory is divided into three equal zones, with only 6 GCP's, IBN/GPS-DP helps to provide OSC's with averaged absolute error of 0.135 m and 0.22 m in horizontal and vertical, respectively for the first and last 5 Km, and averaged absolute error of 0.39 m and 0.61 m, respectively for the middle 5 Km.

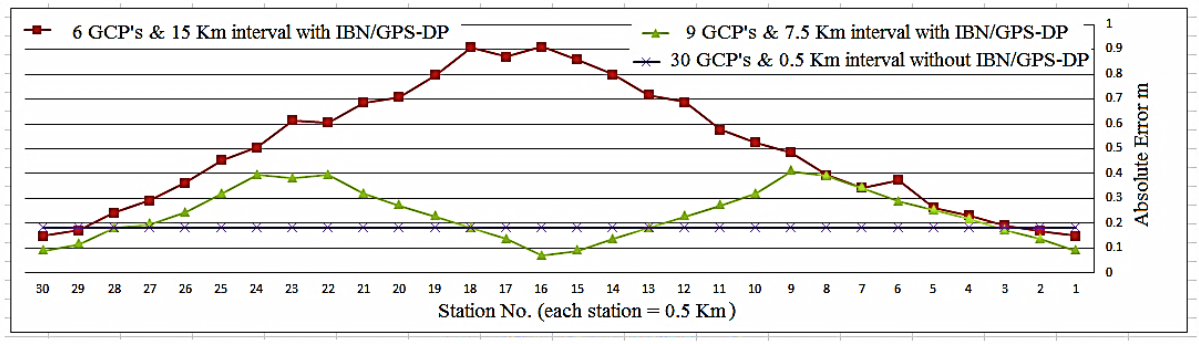

Figure 2: The absolute errors of check points with GCP's intervals of 15 Km, 7.5 Km & 0.5 Km

With 9 GCP's, distributed as 3 equal groups with intervals of 7.5 Km, the integration of IBN/GPS-DP has helped to improve the quality considerably, providing OSC's with maximum horizontal and vertical absolute error of 0.29 m and 0.41 m, respectively and averaged absolute error of 0.13 m & 0.19 m, respectively along the route. The absolute error near the GCP's areas reduce considerably, averaging about 0.07 m and 0.10 m for horizontal and vertical, respectively. This quality obtained from the integration of IBN/GPS-DP with only well-distributed 9 GCP's is very close to the that obtained from the typical photogrammetric processing applied in [4] with 30 GCP's distributed well along the pipeline route. This can be referred mainly to the high-importance of providing the typical photogrammetric solutions with controlled and accurate positioning for the capturing centers alone the trajectory, with precise standard deviations, which may not be possible with the conventional degraded stand-alone GPS code positioning utilized in low-cost drones.

V. CONCLUSION & RECOMMENDATIONS

In this paper, the integration of IBN/GPS-DP has been investigated, tested and evaluated for enhancing low-cost drone navigation and reducing the number of GCP's required for robust SCBBA. The whole processed data in this paper has been based on previous applied project, in which 98 overlapped aerial images, taken from 350 m height with 8 cm ground pixel footprint have been captured for covering nearly 15 km route. The site is an empty desert area located in the South of Libya and fully with sand dunes that fluctuate in elevations significantly. DJI Mavic 2 PRO drone, with Hasselblad L1D-20C 20 MP camera & UHD video has been used for carrying out the flight mission. The drone has been provided by additional u-blox GPS receiver for recording GPS carrier phase observations. Self-developed Matlab algorithms, LGO and LPS software has been used for carrying out the suggested integration, processing the collected data, and evaluating the results. Different number of GCP's and intervals have been used for evaluation the capability of the IBN/GPS-DP integration for reducing the need of GCP's along the trajectory. This has included utilizing only 6 GCP's, distributed as 3 GCP's at the beginning and the rest by the end of the trajectory after 15 Km, and 9 GCP's, distributed as 3 equal groups with intervals of 7.5 Km. The obtained results of these two trails have been compared to the quality of the OSC's that achieved using 30 GCP's distributed well along the route without the integration of IBN/GPS-DP.

The results show that utilizing the integration of IBN/GPS-DP has in general reduced significantly the high-need of GCP's along the trajectory for low-cost drones. The quality of check points with only 9 GCP 's, distributed as 3 equal groups along the route with interval of 7.5 Km, has been very similar to that obtained without the integration of IBN/GPS-DP using 30 well-distributed GCP's with interval of 0.5 Km. Tests show that the quality of OSC's decreases with increasing the distance from the GCP's, reaching the minimum nearly in the middle of intervals. With 15 Km interval between GCP's, the quality of OSC's has been relatively degraded, especially in the middle of trajectory, where the two integrated techniques are error-cumulative and based only on GCP's to band the drifts. For increasing the quality of the results, reducing the required number of GCS's, and increasing the GCS's intervals, it is recommended to increase the quality of the aerial images using higher camera resolutions, bigger focal lengths, smaller pixel sizes, and less flying height. These factors can help to improve precision of the automatic image matching, providing more accurate image coordinates, and as a consequence, more precise IBN can be achieved. Also, carrier phase GPS+GLONASS observables can be used instead of that of GPS alone, which can help for providing more reliable and dependable delta positioning. SCBBA with additional camera calibration parameters can also be investigated for more precise results, where this can help to enhance the quality of image coordinates. Finally, the integration of IBN/GPS-DP has shown a good ability to reduce significantly the high-need of GCP's in aerial triangulation using low-cost drones, which helps to reduce the cost, effort, and time, and carry out the aerial photogrammetric works in inaccessible or partially accessible areas.

REFERENCES

[1] McGlone J, Mikhail E, Bethel J, Roy M. Manual of photogrammetry. 5th ed. Bethesda Md: American Society of Photogrammetry and Remote Sensing; 2004.

[2] Amami M. Low Cost Vision Based Personal Mobile Mapping System [Ph.D. dissertation]. University of Nottingham, UK; 2015.

[3] Amami M, Elmehdwi A, Borgaa A, Buker A, Alareibi A. Investigations into utilizing low-cost amateur drones for creating ortho-mosaic and digital elevation model. International research journal of modernization in engineering technology and science. March 2022; 4(3): 2107-2118.

[4] Amami M, EL-Turki A, Rustum A, EL-Amaari I, Jabir T. Topographic Surveying using low-cost amateur drones & 4K ultra-high-definition videos. Open Access Research Journal of Science and Technology. April 2022; 4(2): 072-082.

[5] Amami M, Smith M, Kokkas N. Low Cost Vision Based Personal Mobile Mapping System. ISPRS- International Archives of The Photogrammetry, Remote Sensing and Spatial Information Sciences. 2014; XL-3/W1: 1-6.

[6] Amami M. Fast and Reliable Vision-Based Navigation for Real Time Kinematic Applications. International Journal for Research in Applied Sciences and Engineering Technology. Feb. 2022; 10(2): 922-932.

[7] Amami M. The Advantages and Limitations of Low-Cost Single Frequency GPS/MEMS-Based INS Integration. Global Journal of Engineering and Technology Advances. Feb. 2022; 10(2): 018-031.

[8] Amami M. Testing Patch, Helix and Vertical Dipole GPS Antennas with/without Choke Ring Frame. International Journal for Research in Applied Sciences and Engineering Technology. Feb. 2022; 10(2): 933-938.

[9] Amami M. Enhancing Stand-Alone GPS Code Positioning Using Stand-Alone Double Differencing Carrier Phase Relative Positioning. Journal of Duhok University (Pure and Eng. Sciences). 2017; 20(1): 347-355.

[10] Amami M. The Integration of Time-Based Single Frequency Double Differencing Carrier Phase GPS/ Micro-Elctromechanical System-Based INS. International Journal of Recent Advances in Science and Technology. Dec. 2018; 5(4): 43-56.

[11] Amami M. A Novel Design Concept of Cost-Effective Permanent Rail-Track Monitoring System. World Journal of Advanced Research and Reviews. March 2022; 13(3): 451-473.

[12] Amami M. The Integration of Stand-Alone GPS Code Positioning, Carrier Phase Delta Positioning & MEMS-Based INS. International Research Journal of Modernization in Engineering Technology and Science. March 2022; 4(3): 700-715.

[13] Amami M. Speeding up SIFT, PCA-SIFT & SURF Using Image Pyramid. Journal of Duhok University, [S.I]. July 2017; 20(1): 356-362.

[14] Amami M. Multi and Single Epipolar Geometry-Based Filters Vs. Affine and Conformal 2D Transformation-Based Filters. Global Journal of Engineering and Technology Advances. March 2022; 10(3): 032-051.

[15] Amami M. Comparison Between Multi & Single Epipolar Geometry-Based Filters for Optical Robot Navigation. International Research Journal of Modernization in Engineering Technology and Science. March 2022; 4 (3): 476-485.

[16] Amami M. Comparison Between Multi Epipolar Geometry & Conformal 2D Transformation-Based Filters for Optical Robot Navigation. International Journal for Research in Applied Sciences and Engineering Technology. March 2022; 10(3): 388-398.

[17] Amami M. Comparison Between Multi Epipolar Geometry & Affine 2D Transformation-Based Filters for Optical Robot Navigation. International Journal for Research in Applied Sciences and Engineering Technology. March 2022; 10(3): 399-409.